



OPEN ACCESS

EDITED BY
Matheus Mattos,
KU Leuven, Belgium

REVIEWED BY
Krishnamurthy Genasan,
University of Malaya, Malaysia
Paramita Chatterjee,
Georgia Institute of Technology, United States

*CORRESPONDENCE
Weiquan Zeng
✉ fujianwys@126.com
Jian Li
✉ lijianla2008@foxmail.com

†These authors have contributed equally to this work and share first authorship

RECEIVED 08 April 2025
ACCEPTED 10 June 2025
PUBLISHED 25 June 2025

CITATION
Wu Y, Liu J, Yu W, Wang X, Li J and Zeng W (2025) Single-cell transcriptome and multi-omics integration reveal ferroptosis-driven immune microenvironment remodeling in knee osteoarthritis.
Front. Immunol. 16:1608378.
doi: 10.3389/fimmu.2025.1608378

COPYRIGHT
© 2025 Wu, Liu, Yu, Wang, Li and Zeng. This is an open-access article distributed under the terms of the [Creative Commons Attribution License \(CC BY\)](https://creativecommons.org/licenses/by/4.0/). The use, distribution or reproduction in other forums is permitted, provided the original author(s) and the copyright owner(s) are credited and that the original publication in this journal is cited, in accordance with accepted academic practice. No use, distribution or reproduction is permitted which does not comply with these terms.

Single-cell transcriptome and multi-omics integration reveal ferroptosis-driven immune microenvironment remodeling in knee osteoarthritis

Yushun Wu ^{1†}, Jing Liu ^{2†}, Wenyong Yu³, Xiaoding Wang ⁴, Jian Li^{1*} and Weiquan Zeng ^{5*}

¹Department of Sports Medicine, The Second Affiliated Hospital of Fujian University of Traditional Chinese Medicine, Fuzhou, China, ²Department of Pain Management, The Affiliated Hospital of Fujian University of Traditional Chinese Medicine, Fuzhou, China, ³The First Clinical Medical College, Fujian University of Traditional Chinese Medicine, Fuzhou, China, ⁴College of Computer and Network Space Security, Fujian Normal University, Fuzhou, China, ⁵Department of Orthopedics, The Rehabilitation Hospital of Fujian University of Traditional Chinese Medicine, Fuzhou, China

Background: Knee osteoarthritis (KOA) is a chronic inflammatory joint disorder marked by cartilage degradation and immune microenvironment dysregulation. While transcriptomic studies have identified key pathways in KOA, the interplay between ferroptosis (an iron-dependent cell death mechanism) and immune dysfunction at single-cell resolution remains unexplored. This study integrates single-cell and bulk transcriptomics to dissect ferroptosis-driven immune remodeling and identify diagnostic biomarkers in KOA.

Methods: We analyzed scRNA-seq data (GSE255460, $n = 11$) and bulk RNA-seq cohorts (GSE114007: 20 KOA/18 controls; GSE246425: 8 KOA/4 controls). Single-cell data were processed via Seurat (QC: mitochondrial genes >3 MAD; normalization: LogNormalize; batch correction: Harmony) and annotated using CellMarker/PanglaoDB. CellChat decoded intercellular communication, SCENIC reconstructed transcriptional networks, and Monocle2 for pseudotime trajectory mapping. Immune infiltration (CIBERSORT) and a LASSO-SVM diagnostic model were validated by ROC curves. Functional enrichment (GSEA/GSVA) and immunometabolic profiling were performed.

Results: Twelve chondrocyte clusters were identified, including ferroptosis-active homeostasis chondrocytes (HomC) ($p < 0.01$), which exhibited 491 DEGs linked to lipid peroxidation. HomC orchestrated synovitis via FGF signaling (ligand-receptor pairs: FGF1-FGFR1), amplifying ECM degradation and inflammatory cascades (CellChat). SCENIC revealed 10 HomC-specific regulons (e.g., *SREBF1*, *YY1*) driving matrix metalloproteinase activation. A 7-gene diagnostic panel (*IFT88*, *MIEF2*, *ABCC10*, etc.) achieved AUC = 1.0 (training) and 0.78 (validation). Immune profiling showed reduced resting mast cells ($p = 0.003$) and monocytes ($p = 0.02$), with *ABCC10* correlating negatively with CD8+ T cells ($r = -0.65$) and M1 macrophages. GSEA/GSVA implicated HIF-1, NF- κ B, and oxidative phosphorylation pathways in KOA progression. Pseudotime analysis revealed fibrotic transitions (*COL1A1*↑, *TNC*↑) in late-stage KOA cells.

Conclusion: This study establishes ferroptosis as one of the key drivers immune-metabolic dysfunction in KOA, with HomC acting as a hub for FGF-mediated synovitis and ECM remodeling. The diagnostic model and regulon network (*SREBF1/YY1*) offer translational tools for early detection, while impaired mast cell homeostasis highlights novel immunotherapeutic targets. Our findings bridge ferroptosis, immune dysregulation, and metabolic stress, advancing precision strategies for KOA management.

KEYWORDS

knee osteoarthritis, ferroptosis, single-cell transcriptomics, immune microenvironment, diagnostic biomarkers

1 Introduction

Knee osteoarthritis (KOA) is a chronic inflammatory disease of the joint, characterized by degenerative changes in cartilage and dysregulation of the immune microenvironment (1, 2). KOA has a major adverse impact on patients' quality of life and poses a considerable economic burden on healthcare systems globally (3, 4). Current management strategies of KOA comprise medications across various pharmacological classes, physical interventions, and surgical procedures, which often show limited treatment efficacy with varying adverse effects (5, 6). This exemplifies the urgent need to develop new treatment approaches for KOA.

The recent use of transcriptomic approaches have generated valuable information regarding gene expression profiles in KOA, noting inflammatory pathways and immune cell infiltration as contributors to disease progression (7, 8). However, these studies mostly examine bulk tissue samples which mask the cellular heterogeneity in the joint and do not illustrate the complex cell-specific interactions that drive immune remodeling in KOA (9, 10). At a cellular level, a number of types of immune cells, such as macrophages, mast cells, and T-lymphocytes, may interact in the synovial microenvironment to drive inflammation and matrix degradation (11–13).

Ferroptosis, a form of iron-dependent regulated cell death, has emerged as a critical mechanism in various diseases, including osteoarthritis (14, 15). This process is characterized by lipid peroxidation and oxidative stress, both of which are central to the pathophysiology of KOA (16, 17). Despite its significance, the role of ferroptosis in immune microenvironment remodeling and cartilage degradation in KOA has not been explored in detail, particularly at the single-cell level.

To address this knowledge gap, we combine single-cell RNA sequencing (scRNA-seq) and bulk transcriptomic data to provide a multi-faceted overview of the immune microenvironment in KOA. This multi-omics approach allows us to examine the interplay of ferroptosis and immune dysregulation in KOA. The distinguishing feature of scRNA-seq is its ability to demonstrate cell heterogeneity and the subpopulations of immune cells that may be involved in the

pathogenic processes to an increasing degree of resolution (18, 19). This will allow for a greater understanding of how ferroptosis impacts immune remodeling and contributes to disease progression (20).

The primary aim of this study is to identify biomarkers associated with ferroptosis driven immune microenvironment remodeling in KOA. These biomarkers have the potential to be used as early diagnostic tools and as targets for therapeutic intervention for new treatment approaches (21). The hope is that an enhanced understanding of the molecular mechanisms occurring in KOA will provide new insights into disease pathogenesis, as well as provide new therapeutic avenues for the development of more efficacious treatments for KOA.

2 Methods

2.1 Data acquisition

GEO database (<https://www.ncbi.nlm.nih.gov/geo/info/datasets.html>) the full name of GENE EXPRESSION OMNIBUS, is by the us national center for biotechnology information (NCBI) database creation and maintenance of GENE EXPRESSION. To ensure clarity, we explicitly detail the origin and characteristics of each dataset used in this study. GSE255460 comprises single-cell RNA sequencing data from human knee articular cartilage tissue of 11 patients with KOA. The annotation platform was GPL24676, and batch effect correction was performed using the Harmony algorithm. GSE114007 consists of bulk mRNA expression data from knee articular cartilage tissue, including 20 samples from OA patients and 18 samples from healthy controls, and served as the model training set. GSE246425 provides mRNA expression profiles of *in vitro* cultured human chondrocytes, incorporating samples from both OA patients and healthy donors; chondrocytes were cultured to replicative senescence (Hayflick limit) to establish a senescent cell model. This dataset, also annotated with GPL24676, was used as a validation cohort and comprised 8 OA samples and 4 control samples. Notably, both GSE255460 and GSE114007 were sourced from knee cartilage tissue, whereas GSE246425 was derived

from isolated chondrocytes cultured *in vitro*. For all differential analyses involving two groups, the Wilcoxon test was employed. Since only two groups (control vs. OA) were compared, ANOVA was not applied. Detailed inclusion and exclusion criteria, OA severity grading, sample collection, and single-cell isolation methods for GSE255460 are available in the original publication. All data were derived from publicly available datasets with original ethical approvals documented in the primary studies.

2.2 Single cell data quality control

The expression profile was first read through the Seurat packet, in which we filtered the cells according to the total UMI per cell, the number of genes expressed (22), and the proportion of mitochondrial expression per cell. The proportion of mitochondrial gene expression refers to the percentage of the total expression of mitochondrial genes in the total expression of all genes. Cells with a high proportion of mitochondrial gene expression and a low amount of RNA expression are entering the death process. For rigorous quality control, we employed the median absolute deviation (MAD) method. Variables (such as UMI counts, gene numbers, or mitochondrial content) exceeding 3 MADs from the median were identified as outliers and excluded from downstream analyses. Multiple-testing correction in differential expression analysis was performed using the Benjamini-Hochberg method to control the false discovery rate (FDR).

2.3 Single cell data dimensionality reduction clustering and cell annotation

We adopt the globally standardized LogNormalize method, by multiplying a coefficient s_0 , the total expression of each cell is adjusted to 10000, and then logarithm is taken for standardization. Cell cycle score was calculated using CellCycleScoring. FindVariableFeatures Looks for highly variable genes; We used ScaleData function to remove gene expression fluctuations caused by different mitochondrial gene expression proportion, ribosomal gene expression proportion and cell cycle. The expression matrix was reduced linearly by RunPCA, and principal components were selected for subsequent analysis. The batch effect was removed by Harmony, and the non-linear dimensionality reduction was performed by RunUMAP Unified Manifold Approximation and Projection (UMAP). By searching CellMarker and PanglaoDB database and literature mainly (23, 24), supplemented by automated annotation by SingleR software, cell types existing in corresponding tissues and corresponding marker genes were searched for cell annotation.

2.4 Ligand receptor interaction analysis (CellChat)

CellChat is a tool that enables quantitative inference and analysis of intercellular communication networks from single-cell

data (25). CellChat uses network analysis and pattern recognition methods to predict the major signal inputs and outputs of cells and how these cells and signals coordinate functions. In this analysis, we used standardized single-cell expression profiles as input data, and cell subtypes obtained from single-cell analysis were cell information. Cell-related interactions were analyzed, and weights and counts of inter-cell interactions were used to quantify the closeness of interactions, so as to observe the activity and influence of each type of cell in disease.

2.5 SCENIC analysis

SCENIC(single-cell regulatory network inference and clustering) is a method for calculating gene regulatory network reconstruction and cell state identification based on co-expression and motif analysis of single-cell transcriptome data (26). It first identified the set of genes co-expressed with transcription factors through GENIE3, then carried out motif enrichment analysis for each co-expression module, retained significantly enriched motifs, and TF annotation of motifs using the database, and the annotation results were rated as high and low confidence. TF for direct database annotation and homologous gene inference are high confidence results, TF for motif sequence similarity annotation is low confidence results. The genes in the co-expression module are scored with the retained motif, the genes with significantly high scores are identified (understood as the motif is very close to the TSS of these genes), the genes with low scores in the co-expression module are deleted, and the remaining gene set is called regulon. Each regulon is a transcription factor and the set of genes that directly regulate its target genes, and SCENIC's next job is to score each regulon's activity in individual cells. The score is based on the expression value of the gene, the higher the score represents the higher the degree of activation of the gene set, and the resulting activity matrix can identify the cell type and state.

2.6 Construction of prediction model

Lasso regression was used to further construct the prediction correlation model (27). After incorporating the expression value of each specific gene, a risk score formula for each patient was constructed, weighted by its estimated regression coefficient in lasso regression analysis. The score for each patient was calculated according to the risk score formula, and the ROC curve was used to study the accuracy of the model prediction. At the same time, SVM algorithm was used for feature selection of disease diagnostic markers (28). Svm-rfe is a machine learning method based on support vector machines, which seeks the best variables by deleting the feature vectors generated by SVM, and builds a support vector machine model through the "e1071" software package to further identify the diagnostic value of these biomarkers for diseases.

2.7 Immune infiltration

CIBERSORT method is a widely used method to evaluate immune cell types in microenvironment (29). Based on the principle of support vector regression, the expression matrix of immune cell subtypes was deconvolution analyzed. It contains 547 biomarkers that distinguish 22 human immune cell phenotypes, including T cells, B cells, plasma cells, and myeloid cell subsets. In this study, CIBERSORT algorithm was used to analyze patient data, which was used to infer the relative proportion of 22 kinds of immune infiltrating cells, and correlation analysis was conducted for gene expression and immune cell content.

2.8 GSEA analysis

Gene Set Enrichment Analysis (GSEA) was conducted to assess the differences in pathway enrichment among groups (30). In accordance with the expression levels of the specific genes in the samples, samples were assigned to either a high or low expression group and differences between groups were further examined through the GSEA process. The background gene sets were annotation gene sets of version 7.0 downloaded from the MsigDB database and were considered as annotation gene sets of the subtype type pathways. The process involved differential expression analysis of the pathways between the groups. All significantly enriched gene sets, adjusted p value <0.05 , were ranked based upon the consistency scores. GSEA is frequently used to examine the close association of disease classification with biological process significance.

2.9 GSVA analysis

Gene set variation analysis (GSVA) is an unsupervised, non-parametric method for assessing the enrichment of gene sets from transcriptome data (31). GSVA examines the gene set of interest in a cumulative score to convert the gene level change into pathway level change, and then attempts to make biological function assertions about the sample. In this study, gene sets were downloaded from Molecular Signatures Database, and we computed comprehensive scores for each of the gene sets using the GSVA algorithm to assess potential biological functional changes in the different samples.

2.10 Quasi-temporal analysis

Studies at the single-cell level have made it possible to describe transcriptional regulation of complex physiological processes and highly heterogeneous cell populations. These studies contribute to the discovery of genes that recognize specific cell subtypes, genes that mark intermediate states of biological processes, and genes that transition states between two different cell fates. In many single-cell

studies, individual cells perform the gene expression process in an unsynchronized manner, and each cell is a moment of the transcription process being studied. Monocle introduced the strategy of sequencing individual cells within pseudotime (32), using the non-synchronous processes of individual cells to place them on a trajectory corresponding to biological processes such as cell differentiation.

2.11 Statistical analysis

All statistical analyses were conducted using R language (version 4.3.0), with $p < 0.05$ being statistically significant.

3 Results

3.1 Integration of single-cell data and identification of cellular subpopulations

Considering the data quality of multiple samples, the captured outliers of the cells will be filtered. In the end, a total of 74,182 cells were retained, and the violin diagram and scatter diagram after quality control (Supplementary Figures 1A, Figure 1B) were obtained. We then analyzed 2000 highly variable genes and showed the 10 genes with the highest standard deviation among them (Supplementary Figure 1C). Subsequently, the data were standardized, homogenized, PCA and harmony analyzed and processed successively (Supplementary Figures 1D–F). UMAP plots before and after Harmony correction in the Supplementary Figures 1E, F, which demonstrate that cell clustering by batch has been effectively minimized. After dimensionality reduction by unified manifold approximation and projection (UMAP), a total of 18 subgroups are obtained (Figure 1A). The study further annotated each cell subtype. In total, 12 cell types were identified and annotated: preHTC (prehypertrophic chondrocytes), FC (fibrocartilage chondrocytes), EC (effector) chondrocytes), HomC (homeostasis chondrocytes), proC (proliferation chondrocytes), InfC (inflammatory) chondrocytes), HTC (hypertrophic chondrocytes), preInfC (pre-inflammatory chondrocytes), RepC (reparative) There were 12 types of cells, namely chondrocytes, RegC (regulator chondrocytes), preFC (prefibrocartilage chondrocytes) and cycle cells (Figure 1B). The classic marker genes for each of the 12 cell types are shown in a bubble plot (Figure 1C), and the proportions of each cell type are illustrated in Figure 1D.

3.2 Ferroptosis mechanisms and identification of key cell types

Then we gain the iron from iron death database (<http://www.zhounan.org/ferrdb>) death related genes, a total of 484 iron death related genes, AUCell, UCell, singscore, ssGSEA and Add

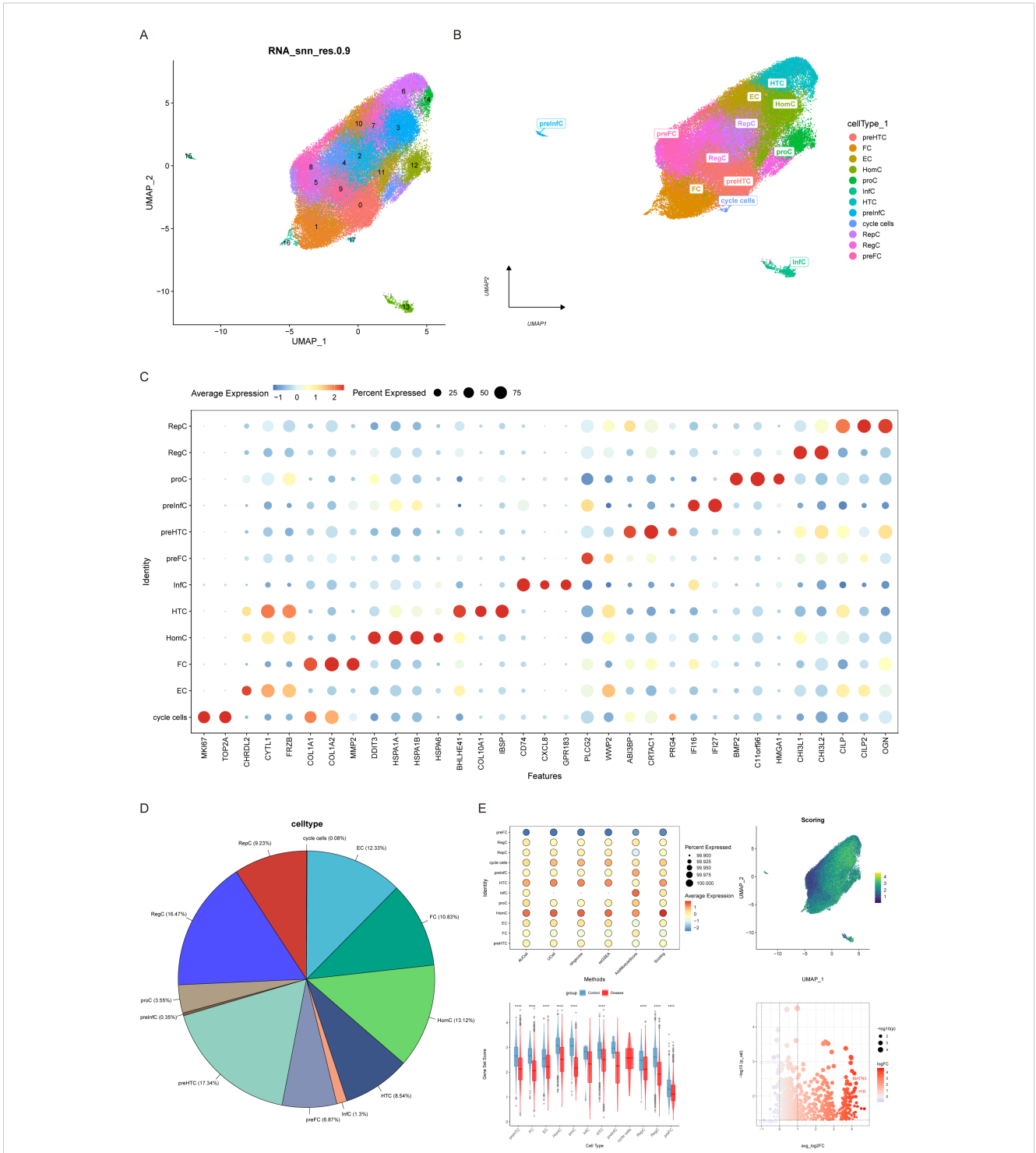


FIGURE 1

Cellular annotation and differences in ferroptosis scores. **(A)** Cells were grouped into 18 clusters using UMAP algorithm based on important components available from PCA. **(B)** Annotation of the 18 clusters, categorized into 12 cell types: preHTC (prehypertrophic chondrocytes), FC (fibrocartilage chondrocytes), EC (effector chondrocytes), HomC (homeostasis chondrocytes), proC (proliferation chondrocytes), IntC (inflammatory chondrocytes), HTc (hypertrophic chondrocytes), preInFC (pre-inflammatory chondrocytes), RepC (reparative chondrocytes), RegC (regulator chondrocytes), preFC (prefibrocartilage chondrocytes), and cycle cells. **(C)** Bubble plot of 12 cell types and their corresponding cell markers in the Doplott. **(D)** Pie chart illustrating the proportion of 12 cell types. **(E)** Differential expression of ferroptosis scores across the 12 cell types.

algorithms were used to evaluate iron death at the level of scRNA-seq, and the scores of the above algorithms were averaged to evaluate the expression of iron death in different cell types. According to the results, the cell subsets with a small number of

cells were eliminated. In the control group and the disease group, the expression of iron death was significantly different in HomC and the total quantified score was the highest in the two groups, so HomC was taken as the key cell (Figure 1E). Subsequently, we

extracted HomC and used pseudo bulk to analyze the difference between the high and low HomC scores according to the median value of its iron death quantization score. The differential gene screening conditions were $p\text{-value} < 0.05$ and $|\log\text{FC}| > 1$. A total of 491 differential genes (Candidate_Genes.txt) were obtained.

3.3 Intercellular communication analysis reveals critical pathways

First, HomC was divided into high-low scores according to quantitative scores. Then, we analyzed the ligand-receptor relationship of feature in single cell expression profile using the software package cellchat. We found complex interaction pairs among these cell subtypes (Figure 2A). Then, we calculated the signal receiving and sending intensity of all cells for all signaling pathways (Figures 2B, C), and found that for HomC, the signal receiving and sending intensity of FGF signaling pathway was higher, pretending to be a critical signaling pathway analysis. Our analysis highlighted the significance of FGF signaling in mediating intercellular communication between HomC and synovial fibroblasts. Scatterplot analysis demonstrated robust FGF-mediated interactions between these cell types (Figure 2D). Chord diagram analysis further identified FGF1-FGFR1 as the most active ligand-receptor pair (Figure 2E), a finding that was corroborated by significantly elevated FGF1 expression in HomC ($P < 0.001$, Figure 2F). Functionally, HomC-derived FGF1 was found to promote the expression of MMP-13 and ADAMTS5 in synovial fibroblasts (Figure 2G), implicating this signaling axis in the degradation of the extracellular matrix (ECM).

3.4 Transcriptional regulatory network reconstruction identifies core regulators

We selected HomC for SCENIC analysis and output all regulatory units in this subpopulation, and we drew a heat map to visualize the regulon activity score for each cell (Figure 3A). We then show the relationship between a gene's Rank and its residual sum of squares (RSS), which reflects the relative importance of each gene in the network. The results showed that SREBF1, DBP, YY1, MXD4, BHLHE41, ZNF135, MSX2, ZNF732, EGR4, TCF4 and other genes ranked first, and the regulator with higher RSS value may be specifically related to this cell population. Through RSS scores, we identified these 10 regulons as key regulatory elements in KOA (Figures 3B, C).

3.5 Multi-omics feature integration and construction of the diagnostic model

We downloaded the dataset of GSE114007 related to KOA from GEO database as the training set, and used the dataset GSE246425 as the validation set, and performed feature screening on 491

differential genes by Lasso regression. The results showed that Lasso regression consensus identified 7 genes as characteristic genes, as key genes for subsequent research, and built a prediction model (Figures 4A–C). The model formula is as follows: $\text{RiskScore} = \text{IFT88} (0.1082) + \text{MIEF2} (0.0795) + \text{STK32B} (0.0356) + \text{KCTD14} (0.0053) + \text{ZNF81} \times 0.0274 + \text{SPTSSB} \times 0.0538 + \text{ABCC10} \times 0.0848$. The results showed that the prediction model constructed by 7 genes had better diagnostic efficiency, and the area under the AUC curve was 1 (Figure 4D). We further verified the diagnostic model against external data sets, and the results showed that the model had strong stability, and the area under the AUC curve of the verification set was 0.7812 (Figure 4E).

3.6 Correlation of model genes with the immune microenvironment

The microenvironment is mainly composed of fibroblasts, immune cells, extracellular matrix, various growth factors, inflammatory factors and special physicochemical characteristics, which significantly affect the diagnosis, survival outcome and clinical treatment sensitivity of diseases. We showed the level distribution of immune infiltrations and the correlation of immune cells in different forms (Figures 5A, B). Compared with the control group, the levels of mast cells resting and monocytes in the samples from the disease group were significantly lower (Figure 5C). We further explored the relationship between key genes and immune cells, and found that IFT88 was significantly positively correlated with mast cells resting and negatively correlated with T cells gamma delta and macrophages M2. MIEF2 was positively correlated with mast cells resting and negatively correlated with Macrophages M2 and Dendritic cells activated. STK32B was positively correlated with mast cells resting and negatively correlated with Macrophages M2. KCTD14 was positively correlated with mast cells resting. ZNF81 was significantly positively correlated with Neutrophils, and negatively correlated with monocytes. SPTSSB was positively correlated with T cells gamma delta. ABCC10 is positively correlated with Macrophages M2 and mast cells activated, and negatively correlated with T cells CD8, Macrophages M1 and mast cells resting (Figure 5D). In addition, we analyzed the associations between key genes and different immune factors, including immunosuppressors, immunostimulators, chemokines, and receptors. These analyses suggest that key genes are closely related to the level of immune cell infiltration and play an important role in the immune microenvironment (Figures 6A–E).

We used AUCCell to quantitatively score genes related to immune metabolism in single cells, and used bubble map to show the differences in the activity of key genes in immune metabolism related pathways. The results showed that SPTSSB, STK32B, ABCC10, ZNF81, KCTD14, IFT88 and MIEF2 were coagulation, mtorc1_signaling, unfolded_protein_response, myc_targets_v1, oxidative_phosphorylation and other pathways have higher activity (Supplementary Figure 2).

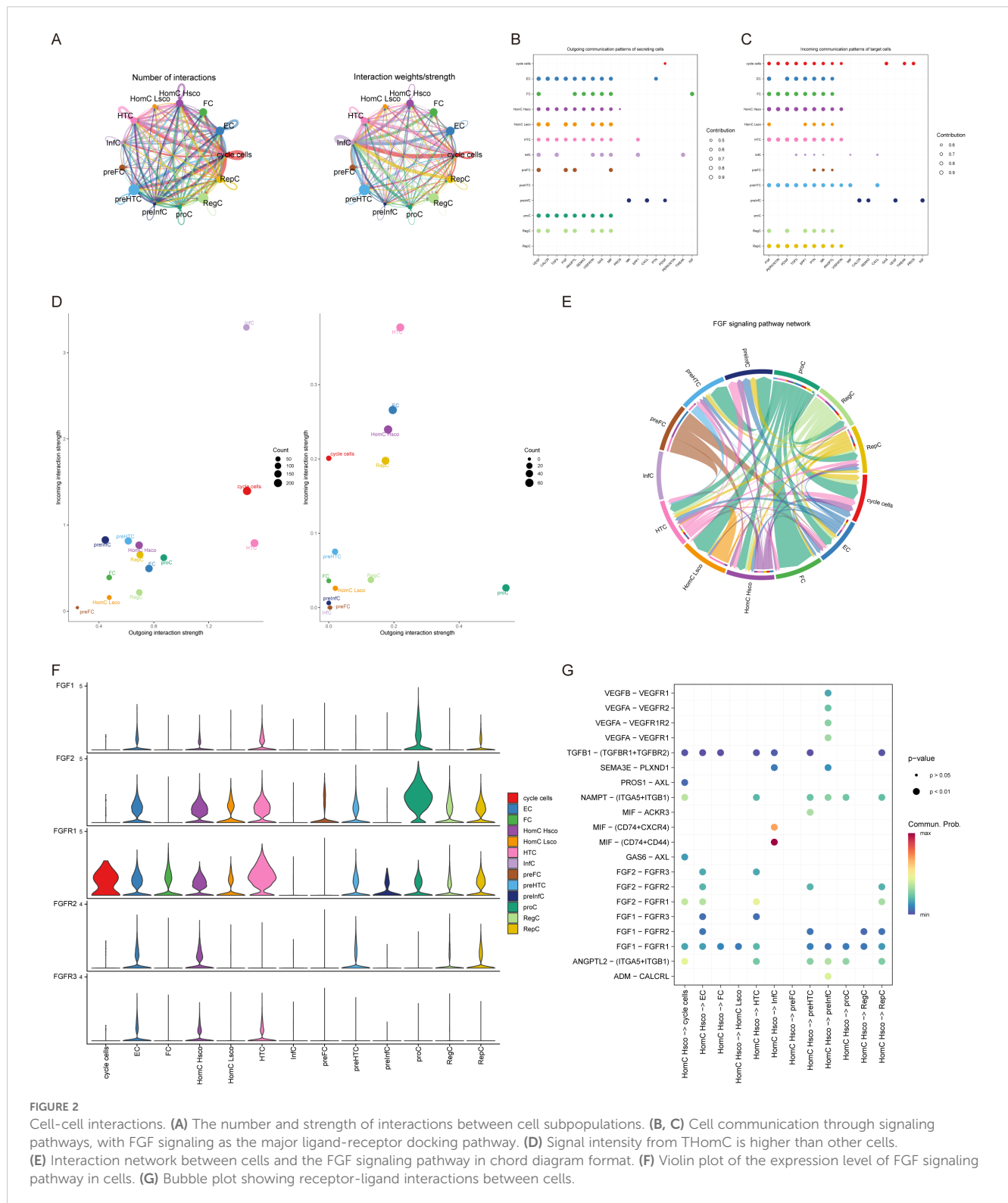


FIGURE 2 Cell-cell interactions. **(A)** The number and strength of interactions between cell subpopulations. **(B, C)** Cell communication through signaling pathways, with FGF signaling as the major ligand-receptor docking pathway. **(D)** Signal intensity from THomC is higher than other cells. **(E)** Interaction network between cells and the FGF signaling pathway in chord diagram format. **(F)** Violin plot of the expression level of FGF signaling pathway in cells. **(G)** Bubble plot showing receptor-ligand interactions between cells.

3.7 Trajectory evolution and functional mechanism validation

Next, we investigate the specific signaling pathways involved in key genes and explore the underlying molecular mechanisms by which key genes influence disease progression. GSEA results

showed that IFT88 was enriched in HIF-1 signaling pathway, Insulin signaling pathway, Notch signaling pathway and other signaling pathways (Figure 7A). MIEF2 is enriched in FoxO signaling pathway, Glucagon signaling pathway, Longevity regulating pathway and other signaling pathways (Figure 7B). STK32B is enriched in HIF-1 signaling pathway, Notch signaling

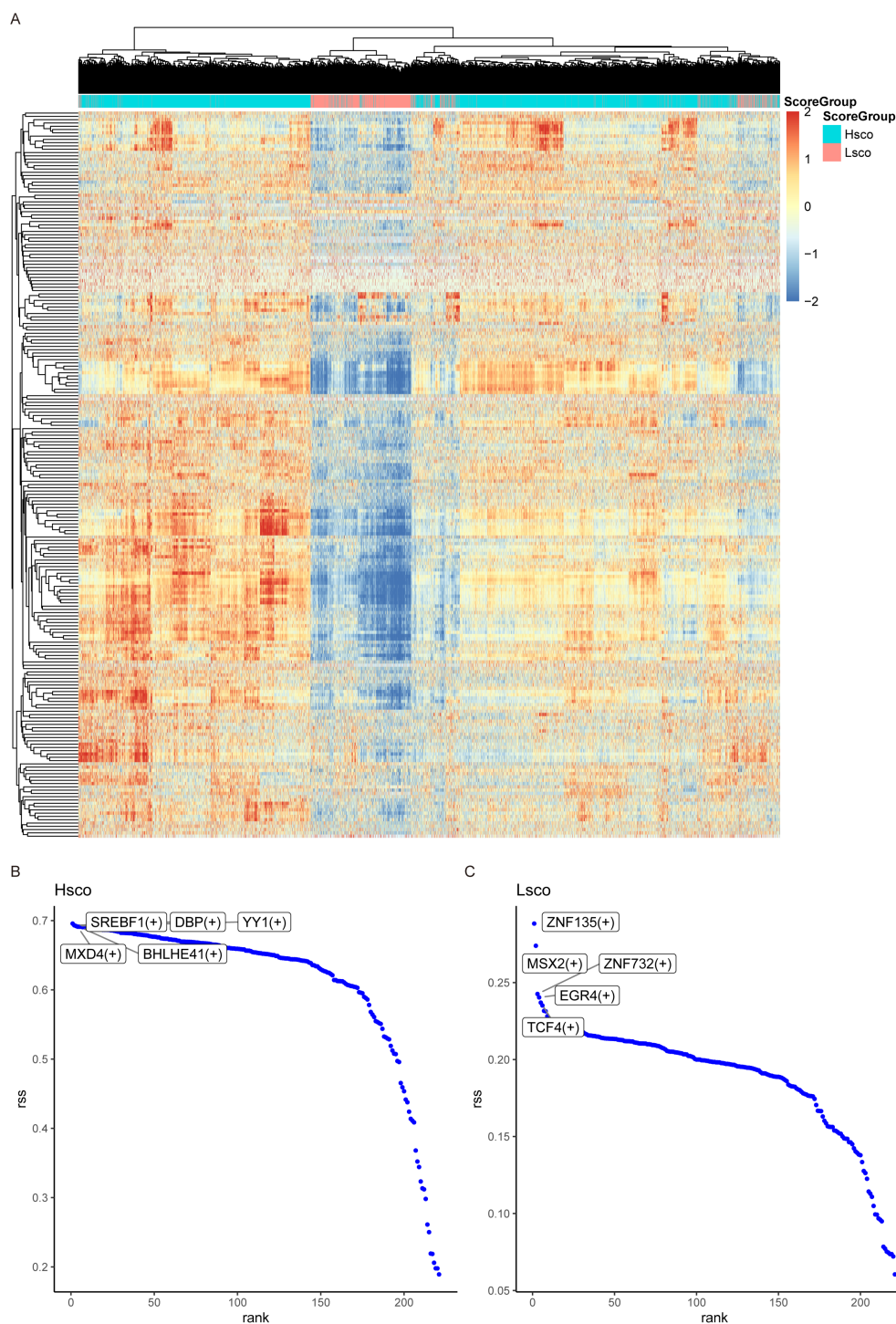
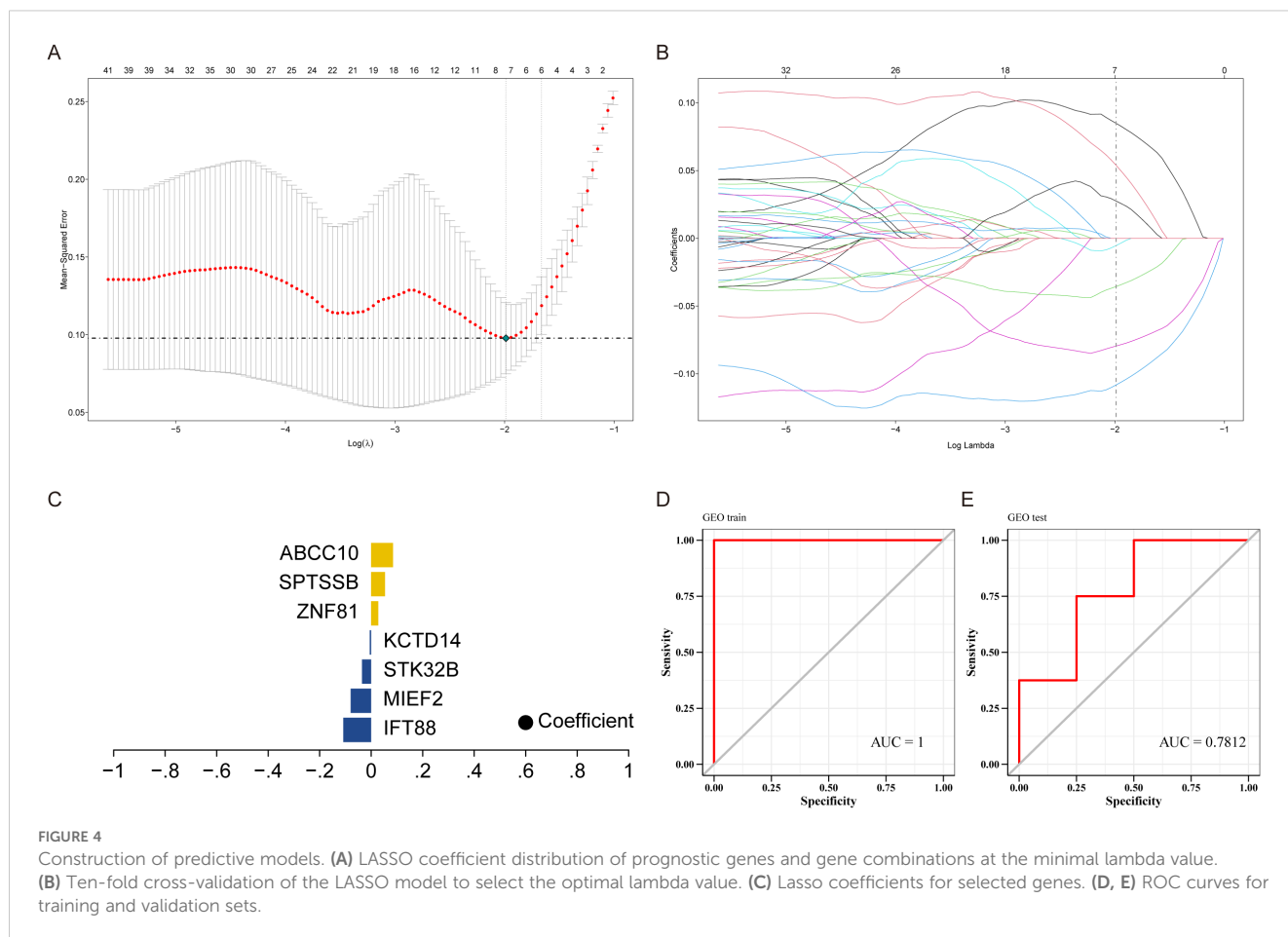


FIGURE 3 SCENIC analysis. **(A)** Heatmap displaying the regulon activity scores of each cell in the HomC subpopulation. SCENIC analysis identified all regulons in this subpopulation, and their activity distribution is visualized. **(B, C)** Scatter plots showing the specificity ranking of transcription factors in high-score and low-score groups.

pathway, AMPK signaling pathway and other signaling pathways (Figure 7C). KCTD14 is enriched in HIF-1 signaling pathway, Notch signaling pathway, IL-17 signaling pathway and other signaling pathways (Figure 7D). ZNF81 is enriched in HIF-1

signaling pathway, Biosynthesis of amino acids, Nucleotide metabolism and other signaling pathways (Figure 7E). SPTSSB is enriched in TGF-beta signaling pathway, PI3K-Akt signaling pathway, N-Glycan biosynthesis and other signaling pathways

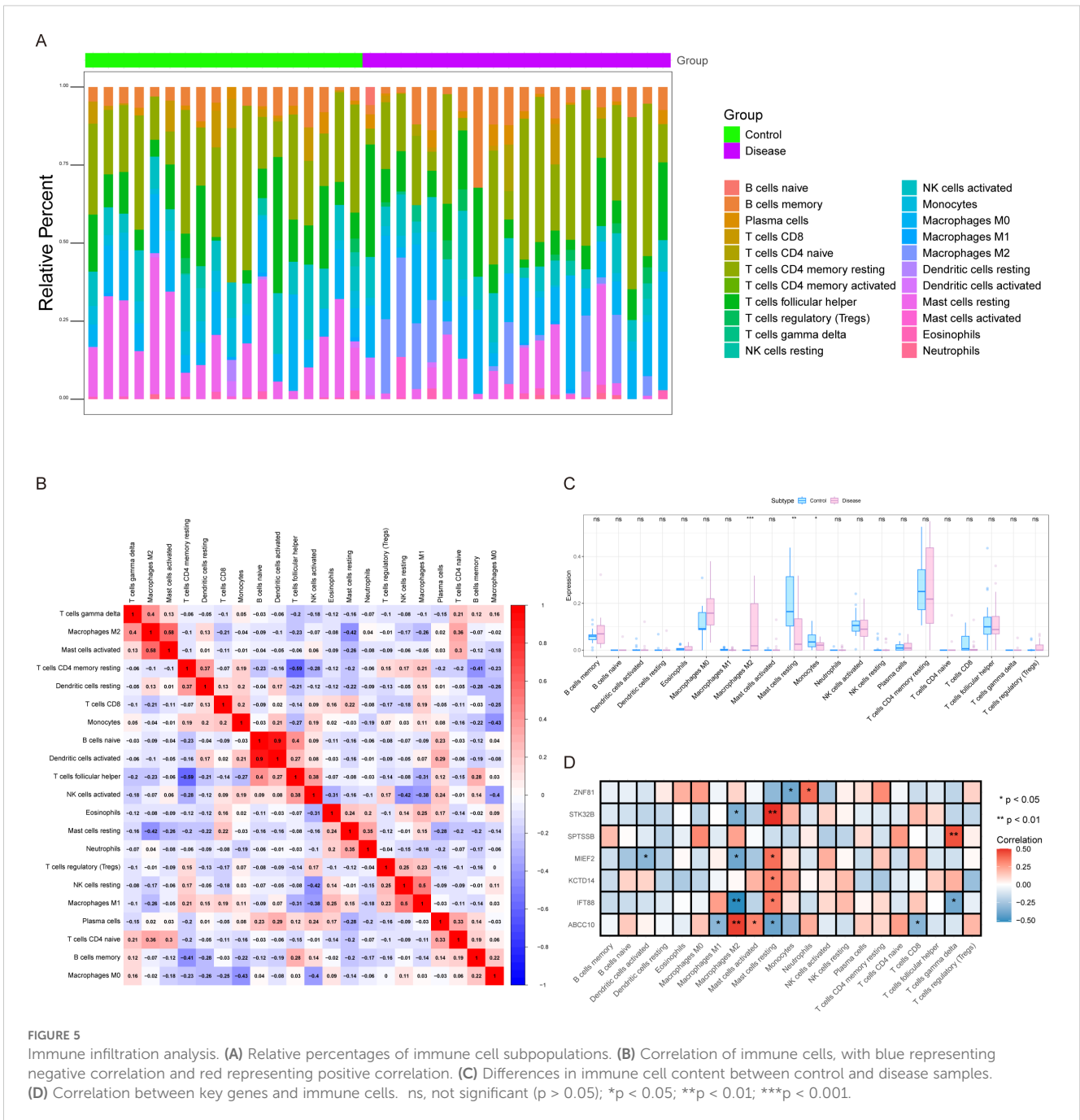


(Figure 7F). ABCC10 is enriched in PI3K-Akt signaling pathway, MAPK signaling pathway, Longevity regulating pathway and other signaling pathways (Figure 7G).

GSVA analysis showed that IFT88 was enriched in TNFA_SIGNALING_VIA_NFKB and NOTCH_SIGNALING pathways (Figure 8A). MIEF2 is enriched in ESTROGEN_RESPONSE_EARLY, TNFA_SIGNALING_VIA_NFKB and other signaling pathways (Figure 8B). STK32B is enriched in NOTCH_SIGNALING, ANGIOGENESIS and other signaling pathways (Figure 8C). KCTD14 is enriched in ANGIOGENESIS, ESTROGEN_RESPONSE_EARLY and other signaling pathways (Figure 8D). ZNF81 is enriched in signal pathways such as UV_RESPONSE_DN and E2F_TARGETS (Figure 8E). SPTSSB is enriched in signal pathways COAGULATION, BILE_ACID_METABOLISM, etc. (Figure 8F). ABCC10 is enriched in signal pathways COAGULATION and EPITHELIAL_MESENCHYMAL_TRANSITION (Figure 8G). This suggests that key genes may influence disease progression through these pathways.

We used the Dotplot, FeaturePlot and VlnPlot functions in the SeuratR package to check the expression of key genes in single cells (Figures 9A, B). Then we carried out a quasi-time series analysis, firstly calculating the similarity between cells and constructing the

cell differentiation trajectory. Then, by visualizing the trajectory, a picture of cell differentiation trajectory constructed in pseudo-time can be generated to show the development process of cells, which can be used to study the process of cell differentiation and gene expression patterns at different time points. pseudotime value (Pseudotime is the probability calculated by monocl based on cell gene expression information, indicating the order of time), state (the block distinguished by path branches) and cell color pictures of different groups were output respectively. The results showed that the control group was mainly distributed in the early stage of cell differentiation. The disease group was mainly distributed in the late stage of cell differentiation (Figures 10A–C). Through the calculation, we also selected and visualized the batch of genes that changed the most along the pseudo-time difference. The horizontal coordinate is the pseudo-time value, and the vertical coordinate is the selected gene, which is divided into 3 clusters by default according to the changes of genes. We found that C2orf40, GGTA1P, FAM129B, KDELC2, SEPT7 and other genes were expressed in the early stage of locus differentiation. COL1A1, TNC, ASPN, COL1A2, S100A4 and other genes were expressed at the end of locus differentiation (Figure 10D). Finally, we also show changes in the expression of key genes during cell differentiation trajectories (Figure 10E).



4 Discussion

KOA is a complex and progressive disease driven by a combination of mechanical, inflammatory, and metabolic factors (33). While extensive research has focused on the inflammatory processes within KOA, the emerging role of non-apoptotic forms of cell death, specifically ferroptosis, in shaping the disease's immune microenvironment is only now beginning to be understood (34, 35). This study provides novel insights into the ferroptosis-driven remodeling of the immune microenvironment in KOA by integrating single-cell transcriptomics with bulk RNA sequencing data. Our findings highlight the critical involvement of ferroptosis

in the pathogenesis of KOA, demonstrating its influence on immune cell polarization, synovial inflammation, and extracellular matrix (ECM) degradation.

The identification of ferroptosis-active homeostasis chondrocytes (HomC) as key players in KOA pathogenesis is a major finding of this study. These cells were found to exhibit significant lipid peroxidation, a hallmark of ferroptosis, and were shown to orchestrate synovitis through fibroblast growth factor (FGF) signaling. Specifically, FGF1 and FGFR1 were identified as ligand-receptor pairs responsible for promoting ECM degradation and inflammation, amplifying the disease process. These results are consistent with previous studies suggesting that ferroptosis

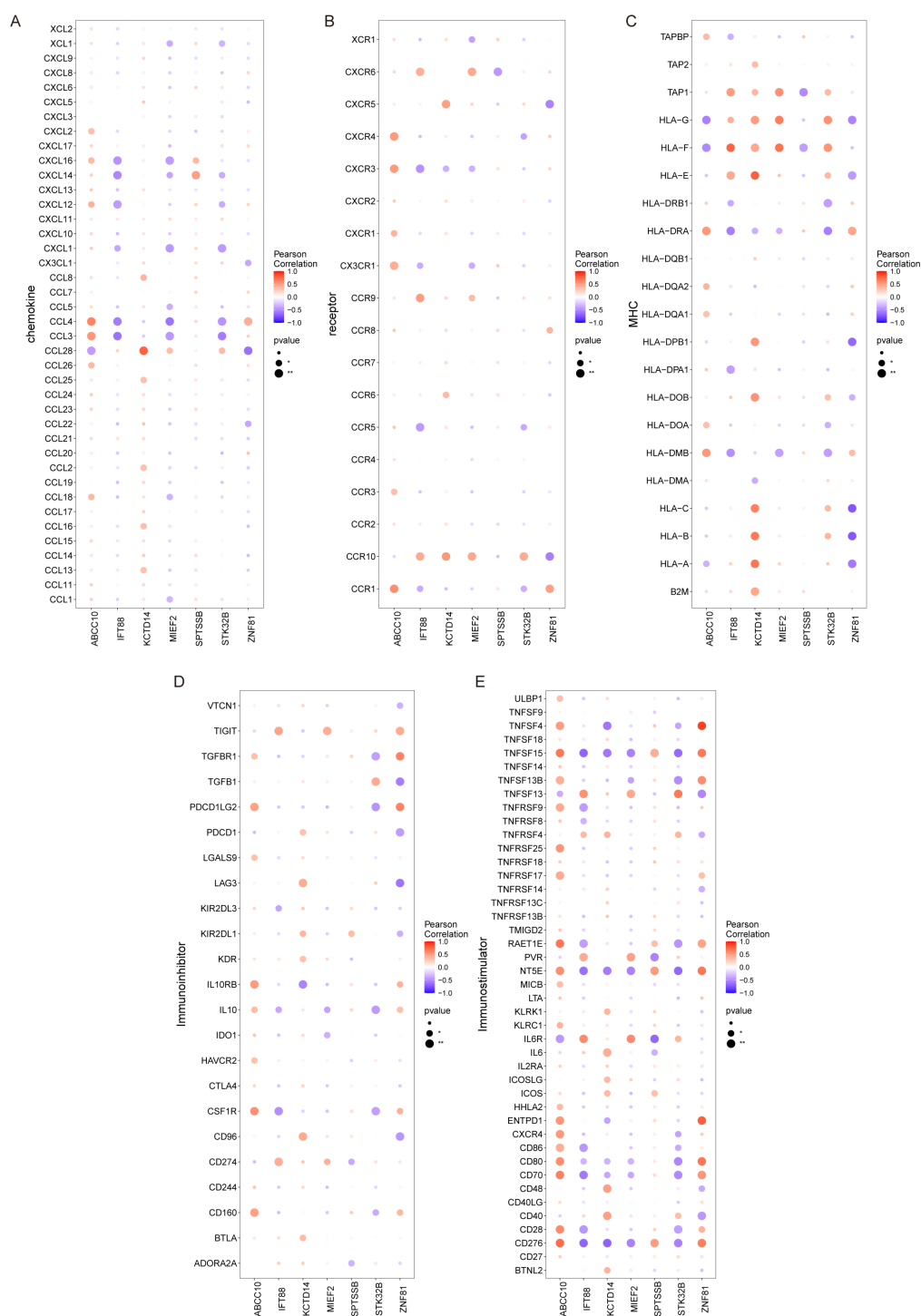


FIGURE 6 Relationship between key genes and immune factors. (A–E) Correlation of key genes with chemokines, immunoinhibitors, immunostimulators, MHC, and receptors.

contributes to tissue damage and inflammation in other models of chronic disease (36, 37), but this is the first study to link it directly with chondrocyte behavior in KOA.

Our analysis using SCENIC revealed that HomC exhibit a unique regulon profile, with transcription factors such as SREBF1

and YY1 driving the activation of matrix metalloproteinases (MMPs). These findings are crucial because MMPs are central to cartilage degradation, and their dysregulation in KOA leads to the breakdown of the ECM, exacerbating joint degeneration (38, 39). This ferroptosis-mediated regulatory network offers a new

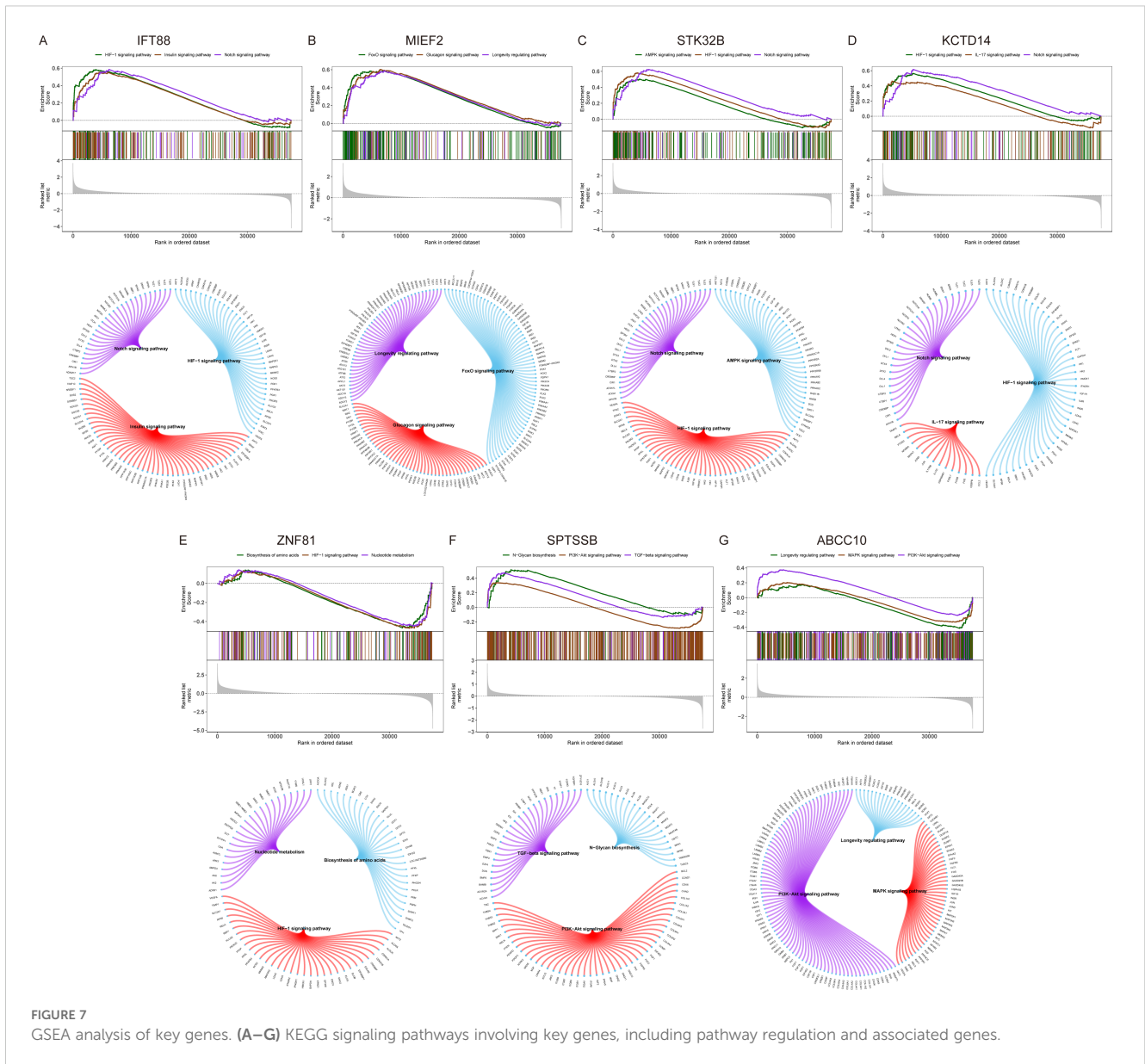


FIGURE 7
 GSEA analysis of key genes. (A–G) KEGG signaling pathways involving key genes, including pathway regulation and associated genes.

perspective on how ferroptotic stress in chondrocytes may be a central mechanism that exacerbates inflammation and tissue degradation, driving KOA progression.

In addition to the direct effects on chondrocytes, we also observed alterations in immune cell profiles within the synovial microenvironment. Specifically, we found reduced resting mast cells and monocytes in KOA, which may indicate an imbalance in immune cell function. The negative correlation between ABCC10 expression and CD8+ T cells as well as M1 macrophages further underscores the interplay between ferroptosis and immune cell activity in KOA (40). This finding suggests that ferroptosis may influence the activation and polarization of immune cells, potentially contributing to the chronic inflammation observed in KOA (41). The role of mast cells, in particular, may be of interest for future research, as their involvement in tissue remodeling and immune modulation could open new avenues for immunotherapeutic interventions (42, 43).

To further explore the cellular dynamics, we employed CellChat and pseudotime trajectory analysis. These approaches revealed that ferroptosis is central to immune ecosystem remodeling in KOA, driving myeloid cell polarization, lymphocyte infiltration, and disruption of stromal-immune metabolic coupling. Our CellChat analysis prioritized the FGF signaling pathway due to its exceptional ligand-receptor intensity in ferroptosis-active homeostasis chondrocytes (HomC) (Figures 2B, C), a finding mechanistically supported by the established role of FGF1–FGFR1 interactions in promoting synovial fibroblast activation, MMP-13 secretion, and extracellular matrix (ECM) degradation (44–46).

Integration with pseudotime trajectory analysis demonstrated that the transition from homeostasis to a fibrotic, inflammatory phenotype in late-stage KOA coincided with elevated FGF1 expression in HomC and increased markers such as COL1A1 and TNC (39, 47). This suggests that ferroptosis-driven FGF signaling

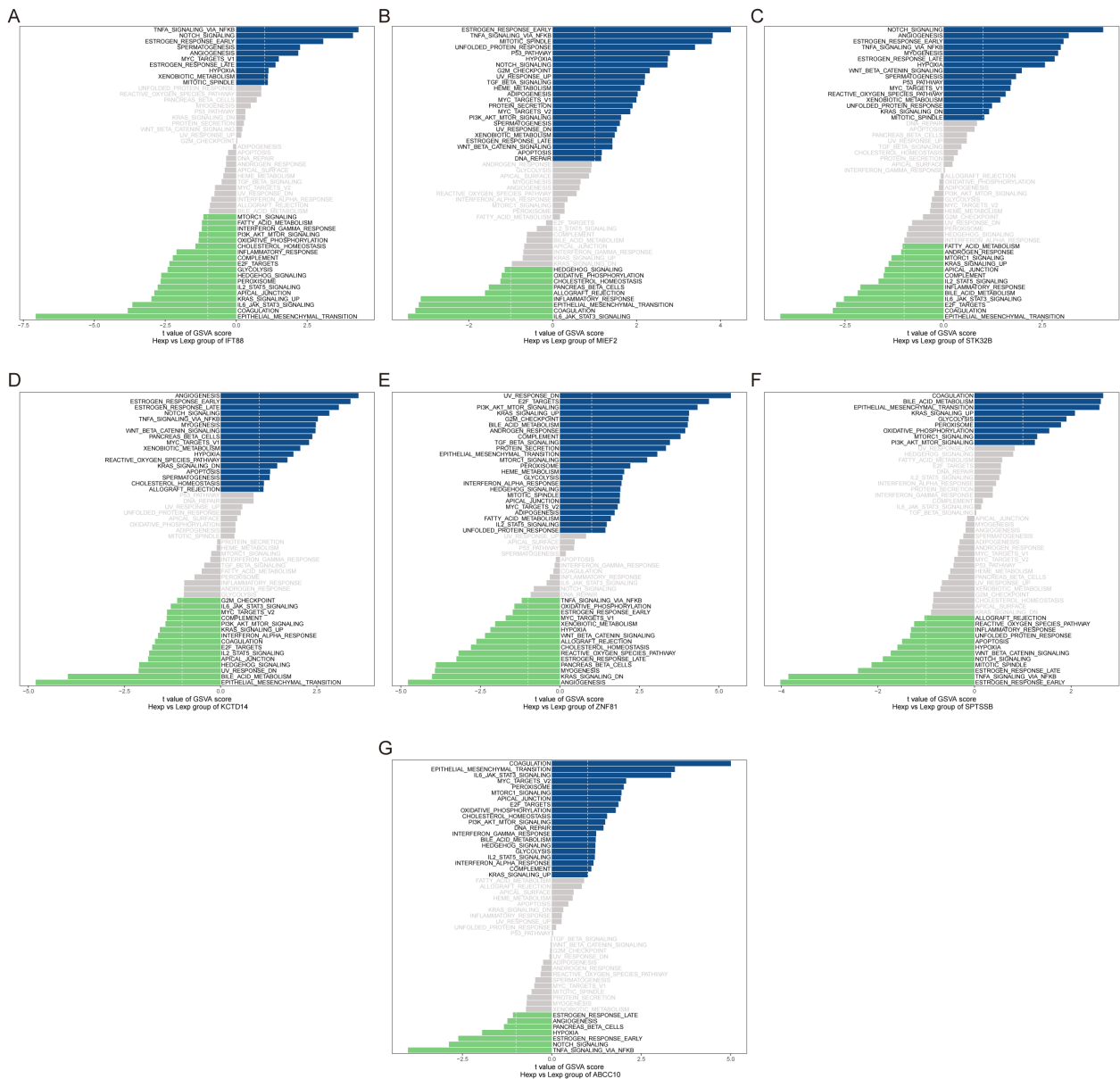


FIGURE 8
GSVA analysis of key genes. (A–G) GSVA analysis for key genes, with blue representing high-expression genes involved in signaling pathways and green representing low-expression genes. The hallmark gene set is used as the background.

amplifies both ECM remodeling and fibrotic reprogramming, linking chondrocyte ferroptosis to synovitis and tissue fibrosis. Collectively, these findings delineate a mechanistic framework in which FGF signaling bridges ferroptosis and immune remodeling in KOA, exacerbating cartilage degradation, inflammation, and fibrosis (48, 49). Furthermore, we observed upregulation of oxidative stress pathways, particularly those regulated by NF-κB and HIF-1, implicating immune-metabolic dysregulation as a central driver of KOA progression (50).

A major strength of this study is the identification of a robust 7-gene diagnostic panel, which achieved an AUC of 1.0 in the training set and 0.78 in the validation cohort. These genes—including IFT88,

MIEF2, and ABCC10—are involved in mitochondrial dynamics, inflammatory response, and iron metabolism (51–54), highlighting their potential for non-invasive early detection of KOA and for guiding future biomarker-based interventions.

In terms of therapeutic applications, our findings point to several potential targets. Ferroptosis inhibitors, which are currently under investigation in cancer therapies (55), could offer a novel approach to modulating cell death in KOA. Targeting immune cell dysfunction, particularly mast cells and macrophages, may help to restore immune balance within the joint and reduce chronic inflammation (56–58). Furthermore, inhibiting the FGF signaling axis—which has been identified as central to HomC-driven synovitis and ECM degradation

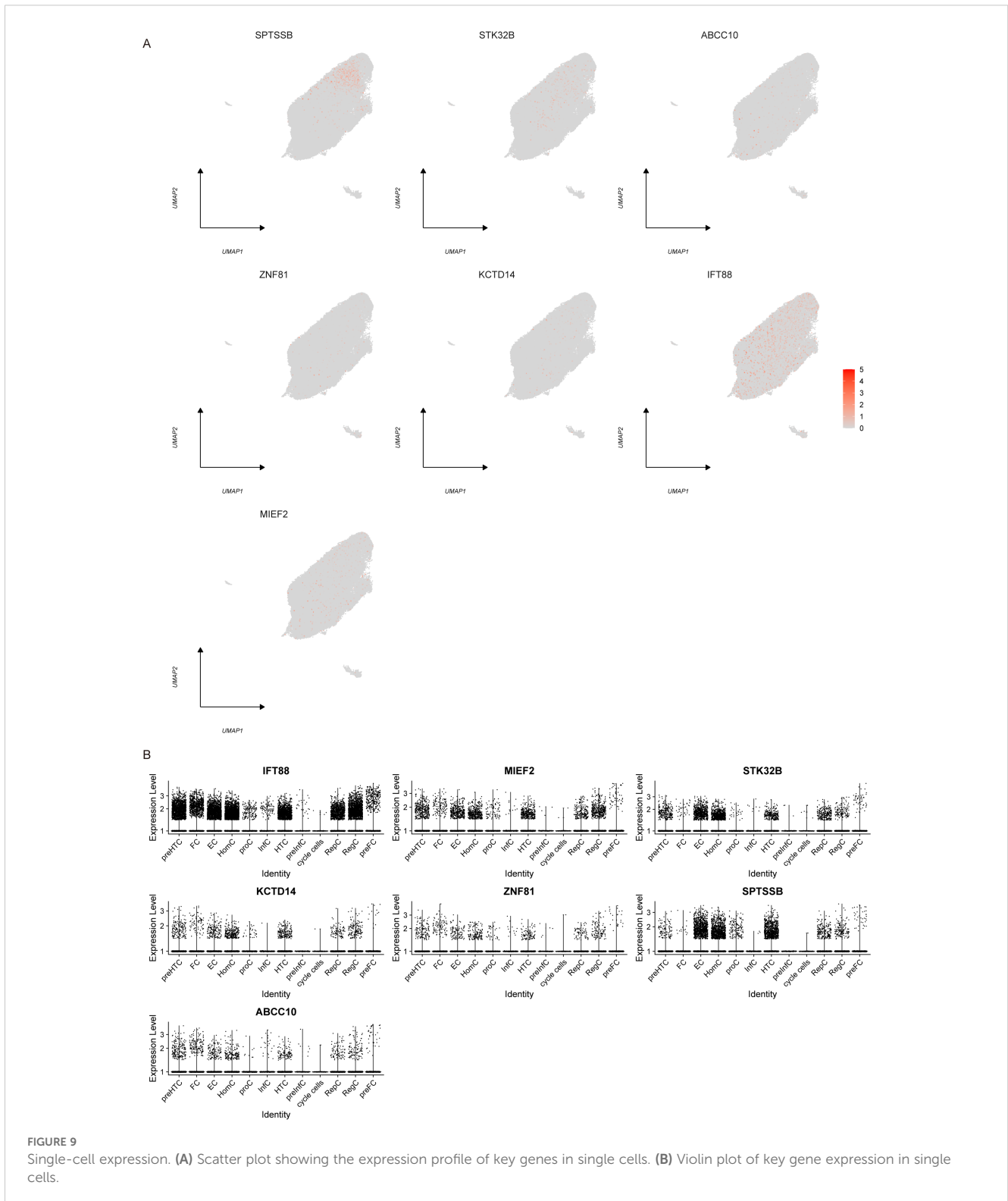
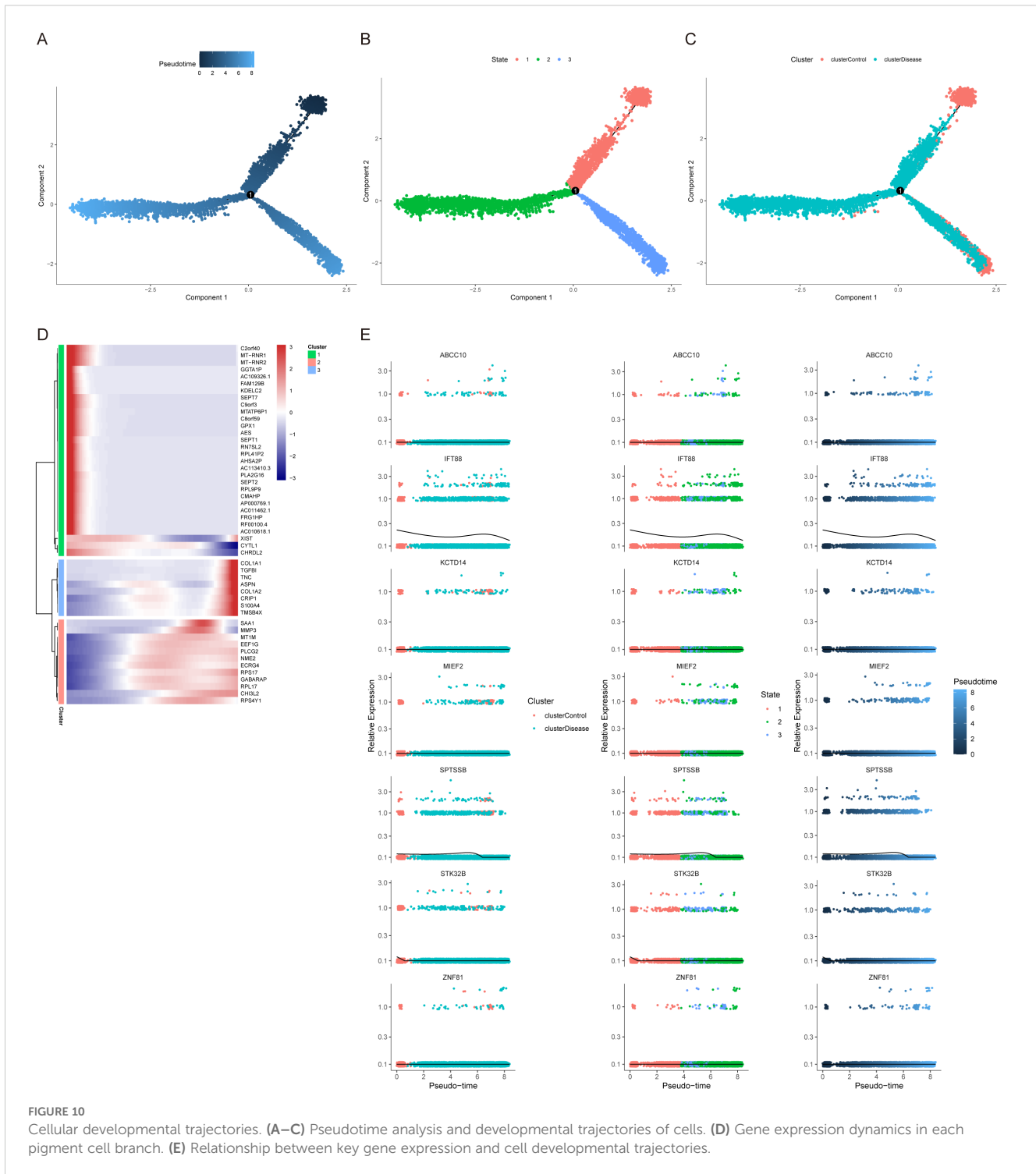


FIGURE 9 Single-cell expression. **(A)** Scatter plot showing the expression profile of key genes in single cells. **(B)** Violin plot of key gene expression in single cells.

—also represents a promising therapeutic strategy. Recent studies, such as that by Xu et al. (59), have further demonstrated that ferroptosis inhibitors can protect chondrocytes while reducing the expression of pro-inflammatory mediators, thereby supporting the therapeutic value of targeting ferroptosis and its associated immunometabolic crosstalk in KOA.

While this study provides valuable insights, several limitations must be considered. First, although batch effect correction for the single-cell RNA-seq data (GSE255460) was performed using the Harmony algorithm and visually assessed by UMAP, quantitative kBET analysis showed only a 2% acceptance rate post-correction, likely due to biological variability and uneven cell type distribution.



Second, the validation cohort was small (GSE246425, n=12), which may limit statistical power and generalizability, and no *a priori* sample size calculation was possible since our work is a secondary analysis of public datasets. Third, all findings are based on computational analysis without direct experimental validation. We have outlined future plans to address this, including lipid peroxidation assays, iron content measurement, and ferroptosis

inhibition experiments. Future studies with larger cohorts and wet-lab experiments are needed to confirm our conclusions and further explore the underlying mechanisms.

Additionally, while the single-cell transcriptomic analysis provides high-resolution data on immune cells and chondrocytes, the spatial organization of these cells within the tissue is not fully addressed. Future studies integrating spatial transcriptomics or immunohistochemistry

could provide more context on how ferroptosis and immune cells interact in the native tissue environment.

Furthermore, while we focused on ferroptosis as a key driver of immune dysfunction in KOA, other forms of non-apoptotic cell death, such as necroptosis or pyroptosis, may also contribute to the disease process. Future studies exploring these pathways could offer a more comprehensive understanding of the molecular mechanisms underlying KOA. Moreover, the role of ferroptosis in other joint diseases, such as rheumatoid arthritis, should be investigated to determine whether the findings in KOA are broadly applicable to other inflammatory conditions.

5 Conclusion

In summary, this study establishes ferroptosis as a key driver of immune-metabolic dysfunction in KOA, linking it to synovitis, ECM remodeling, and disease progression. By integrating single-cell transcriptomics and bulk RNA-seq, we have uncovered novel mechanisms by which ferroptosis influences immune microenvironment remodeling in KOA, providing potential biomarkers and therapeutic targets. Our findings not only enhance the understanding of KOA pathogenesis but also open new avenues for developing precision diagnostic and therapeutic strategies to better manage this debilitating disease.

Data availability statement

The original contributions presented in the study are included in the article/**Supplementary Material**. Further inquiries can be directed to the corresponding authors.

Ethics statement

The studies involving humans were approved by ethics committee of The Second People's Hospital Affiliated to Fujian University of Traditional Chinese Medicine. The studies were conducted in accordance with the local legislation and institutional requirements. The human samples used in this study were acquired from gifted from another research group. Written informed consent for participation was not required from the participants or the participants' legal guardians/next of kin in accordance with the national legislation and institutional requirements.

Author contributions

YW: Conceptualization, Data curation, Formal Analysis, Funding acquisition, Software, Supervision, Validation, Visualization, Writing – original draft. JLi: Conceptualization, Data curation, Formal Analysis, Funding acquisition, Software, Supervision, Validation, Visualization,

Writing – original draft. WY: Data curation, Formal Analysis, Software, Validation, Visualization, Writing – original draft. XW: Data curation, Formal Analysis, Software, Validation, Visualization, Writing – original draft. JLi: Supervision, Writing – review & editing. WZ: Supervision, Writing – review & editing.

Funding

The author(s) declare that financial support was received for the research and/or publication of this article. This research was funded by the Natural Science Foundation of Fujian Province (2024J01735) and the Key Discipline Project of Traditional Chinese Medicine Orthopedics at Fujian University of Traditional Chinese Medicine (XGS2023006).

Acknowledgments

We gratefully acknowledge the Gene Expression Omnibus (GEO) for their public datasets. We also appreciate the R programming language community for the essential tools that facilitated our research.

Conflict of interest

The authors declare that the research was conducted in the absence of any commercial or financial relationships that could be construed as a potential conflict of interest.

Generative AI statement

The author(s) declare that no Generative AI was used in the creation of this manuscript.

Publisher's note

All claims expressed in this article are solely those of the authors and do not necessarily represent those of their affiliated organizations, or those of the publisher, the editors and the reviewers. Any product that may be evaluated in this article, or claim that may be made by its manufacturer, is not guaranteed or endorsed by the publisher.

Supplementary material

The Supplementary Material for this article can be found online at: <https://www.frontiersin.org/articles/10.3389/fimmu.2025.1608378/full#supplementary-material>

References

- Ross M, Zhou Y, English M, Sharplin P, Hirner M. The effect of intra-articular autologous protein solution on knee osteoarthritis symptoms. *Bone Joint J.* (2024) 106-B:907–15. doi: 10.1302/0301-620X.106B9.BJJ-2024-0258.R1
- Mikulikova Z, Gallo J, Manukyan G, Trajerova M, Savara J, Shrestha B, et al. Complexity of synovial fluid-derived monocyte-macrophage-lineage cells in knee osteoarthritis. *Cell Rep.* (2024) 43:115011. doi: 10.1016/j.celrep.2024.115011
- Zhang L, Zhang C, Zhang J, Liu A, Wang P, Xu J. A bidirectional mendelian randomization study of sarcopenia-related traits and knee osteoarthritis. *Clin Interv Aging.* (2023) 18:1577–86. doi: 10.2147/CIA.S424633
- Niu S, Li M, Wang J, Zhong P, Wen X, Huang F, et al. Identify the potential target of efferocytosis in knee osteoarthritis synovial tissue: a bioinformatics and machine learning-based study. *Front Immunol.* (2025) 16:1550794. doi: 10.3389/fimmu.2025.1550794
- Wilson TG, Baghel M, Kaur N, Datta I, Loveless I, Potla P, et al. Circulating miR-126-3p is a mechanistic biomarker for knee osteoarthritis. *Nat Commun.* (2025) 16:2021. doi: 10.1038/s41467-025-57308-5
- Fan X, Sun AR, Young RSE, Afara IO, Hamilton BR, Ong LJY, et al. Spatial analysis of the osteoarthritis microenvironment: techniques, insights, and applications. *Bone Res.* (2024) 12:7. doi: 10.1038/s41413-023-00304-6
- Peters H, Potla P, Rockel JS, Tockovska T, Pastrello C, Jurisica I, et al. Cell and transcriptomic diversity of infrapatellar fat pad during knee osteoarthritis. *Ann Rheum Dis.* (2025) 84:351–67. doi: 10.1136/ard-2024-225928
- Rai MF, Collins KH, Lang A, Maertz T, Geurts J, Ruiz-Romero C, et al. Three decades of advancements in osteoarthritis research: insights from transcriptomic, proteomic, and metabolomic studies. *Osteoarthritis Cartilage.* (2024) 32:385–97. doi: 10.1016/j.joca.2023.11.019
- Pan B, Yao P, Ma J, Lin X, Zhou L, Lin C, et al. Identification of key biomarkers related to fibrocartilage chondrocytes for osteoarthritis based on bulk, single-cell transcriptomic data. *Front Immunol.* (2024) 15:1482361. doi: 10.3389/fimmu.2024.1482361
- Li J, Gui T, Yao L, Guo H, Lin YL, Lu J, et al. Synovium and infrapatellar fat pad share common mesenchymal progenitors and undergo coordinated changes in osteoarthritis. *J Bone Mineral Res.* (2024) 39:161–76. doi: 10.1093/jbmr/zjad009
- Su Sohn H, Won Choi J, Jhun J, Pil Kwon S, Jung M, Yong S, et al. Tolerogenic nanoparticles induce type II collagen-specific regulatory T cells and ameliorate osteoarthritis. *Sci Adv.* (2022) 8:5284. doi: 10.1126/sciadv.abo5284
- Panichi V, Costantini S, Grasso M, Arciola CR, Dolzani P. Innate immunity and synovitis: key players in osteoarthritis progression. *Int J Mol Sci.* (2024) 25:12082. doi: 10.3390/ijms252212082
- Moulin D, Sellam J, Berenbaum F, Guicheux J, Boutet MA. The role of the immune system in osteoarthritis: mechanisms, challenges and future directions. *Nat Rev Rheumatol.* (2025) 21:221–36. doi: 10.1038/s41584-025-01223-y
- Ji P, Zhou Z, Zhang J, Bai T, Li C, Zhou B, et al. Non-apoptotic cell death in osteoarthritis: Recent advances and future. *Biomed Pharmacother.* (2024) 179:117344. doi: 10.1016/j.biopha.2024.117344
- Ru Q, Li Y, Chen L, Wu Y, Min J, Wang F. Iron homeostasis and ferroptosis in human diseases: mechanisms and therapeutic prospects. *Signal Transduct Target Ther.* (2024) 9:271. doi: 10.1038/s41392-024-01969-z
- Zou Z, Hu W, Kang F, Xu Z, Li Y, Zhang J, et al. Interplay between lipid dysregulation and ferroptosis in chondrocytes and the targeted therapy effect of metformin on osteoarthritis. *J Adv Res.* (2024) 69:515–29. doi: 10.1016/j.jare.2024.04.012
- Zhang Y, Li J, Liu J, Gao Y, Li K, Zhao X, et al. Ferroptosis in osteoarthritis: towards novel therapeutic strategy. *Cell Prolif.* (2024) 58:13779. doi: 10.1111/cpr.13779
- Fan Y, Bian X, Meng X, Li L, Fu L, Zhang Y, et al. Unveiling inflammatory and prehypertrophic cell populations as key contributors to knee cartilage degeneration in osteoarthritis using multi-omics data integration. *Ann Rheum Dis.* (2024) 83:926–44. doi: 10.1136/ard-2023-224020
- Guo D, Zhang S, Gao Y, Shi J, Wang X, Zhang Z, et al. Exploring the cellular and molecular differences between ovarian clear cell carcinoma and high-grade serous carcinoma using single-cell RNA sequencing and GEO gene expression signatures. *Cell Biosci.* (2023) 13:139. doi: 10.1186/s13578-023-01087-3
- Tong L, Yu H, Huang X, Shen J, Xiao G, Chen L, et al. Current understanding of osteoarthritis pathogenesis and relevant new approaches. *Bone Res.* (2022) 10:60. doi: 10.1038/s41413-022-00226-9
- Ni S, Yuan Y, Song S, Li X. A double-edged sword with a therapeutic target: iron and ferroptosis in immune regulation. *Nutr Rev.* (2023) 81:587–96. doi: 10.1093/nutrit/nuac071
- Hao Y, Hao S, Andersen-Nissen E, Mauck WM, Zheng S, Butler A, et al. Integrated analysis of multimodal single-cell data. *Cell.* (2021) 184:3573–3587.e29. doi: 10.1016/j.cell.2021.04.048
- Hu C, Li T, Xu Y, Zhang X, Li F, Bai J, et al. CellMarker 2.0: an updated database of manually curated cell markers in human/mouse and web tools based on scRNA-seq data. *Nucleic Acids Res.* (2023) 51:D870–6. doi: 10.1093/nar/gkac947
- Franzén O, Gan LM, Björkegren JLM. PanglaoDB: A web server for exploration of mouse and human single-cell RNA sequencing data. *Database.* (2019) 2019:baz046. doi: 10.1093/database/baz046
- Jin S, Guerrero-Juarez CF, Zhang L, Chang I, Ramos R, Kuan CH, et al. Inference and analysis of cell-cell communication using CellChat. *Nat Commun.* (2021) 12:1088. doi: 10.1038/s41467-021-21246-9
- Aibar S, González-Blas CB, Moerman T, Huynh-Thu VA, Imrichova H, Hulselmans G, et al. SCENIC: Single-cell regulatory network inference and clustering. *Nat Methods.* (2017) 14:1083–6. doi: 10.1038/nmeth.4463
- Friedman J, Hastie T, Tibshirani R. Regularization paths for generalized linear models via coordinate descent. *J Stat Softw.* (2010) 33:1–22. doi: 10.18637/jss.v033.i01
- Huang S, Nianguang CAI, Penzuti Pacheco P, Narandes S, Wang Y, Wayne XU. Applications of support vector machine (SVM) learning in cancer genomics. *Cancer Genomics Proteomics.* (2018) 15:41–51. doi: 10.21873/cgp.20063
- Chen B, Khodadoust MS, Liu CL, Newman AM, Alizadeh AA. Profiling tumor infiltrating immune cells with CIBERSORT. In: *Methods in Molecular Biology.* Humana Press Inc (2018) 1711:243–59. doi: 10.1007/978-1-4939-7493-1_12
- Yu G, Wang LG, Han Y, He QY. ClusterProfiler: An R package for comparing biological themes among gene clusters. *OMICS.* (2012) 16:284–7. doi: 10.1089/omi.2011.0118
- Hänzelmann S, Castelo R, Guinney J. GSEA: gene set variation analysis for microarray and RNA-Seq data (2013). *BMC Bioinformatics.* (2013) 14:7. doi: 10.1186/1471-2105-14-7
- Trapnell C, Cacchiarelli D, Grimsby J, Pokharel P, Li S, Morse M, et al. The dynamics and regulators of cell fate decisions are revealed by pseudotemporal ordering of single cells. *Nat Biotechnol.* (2014) 32:381–6. doi: 10.1038/nbt.2859
- Liu Y, Da W, Xu MJ, Xiao CX, Deng T, Zhou SL, et al. Single-cell transcriptomics reveals novel chondrocyte and osteoblast subtypes and their role in knee osteoarthritis pathogenesis. *Signal Transduct Target Ther.* (2025) 10:40. doi: 10.1038/s41392-025-02136-8
- Qiu Y, Yao J, Li L, Xiao M, Meng J, Huang X, et al. Machine learning identifies ferroptosis-related genes as potential diagnostic biomarkers for osteoarthritis. *Front Endocrinol (Lausanne).* (2023) 14:1198763. doi: 10.3389/fendo.2023.1198763
- Zhuo D, Xiao W, Tang Y, Jiang S, Geng C, Xie J, et al. Iron metabolism and arthritis: Exploring connections and therapeutic avenues. *Chin Med J (Engl).* (2024) 137:1651–62. doi: 10.1097/CM9.00000000000003169
- Jiang X, Stockwell BR, Conrad M. Ferroptosis: mechanisms, biology and role in disease. *Nat Rev Mol Cell Biol.* (2021) 22:266–82. doi: 10.1038/s41580-020-00324-8
- Lan C, Zhou X, Shen X, Lin Y, Chen X, Lin J, et al. Suppression of IRF9 promotes osteoclast differentiation by decreased ferroptosis via STAT3 activation. *Inflammation.* (2024) 47:99–113. doi: 10.1007/s10753-023-01896-1
- Grillet B, Pereira RVS, Van Damme J, Abu El-Asrar A, Proost P, Opdenakker G. Matrix metalloproteinases in arthritis: towards precision medicine. *Nat Rev Rheumatol.* (2023) 19:363–77. doi: 10.1038/s41584-023-00966-w
- Li M, Deng T, Chen Q, Jiang S, Li H, Li J, et al. A versatile platform based on matrix metalloproteinase-sensitive peptides for novel diagnostic and therapeutic strategies in arthritis. *Bioact Mater.* (2025) 47:100–20. doi: 10.1016/j.bioactmat.2025.01.011
- Hao X, Zheng Z, Liu H, Zhang Y, Kang J, Kong X, et al. Inhibition of APOC1 promotes the transformation of M2 into M1 macrophages via the ferroptosis pathway and enhances anti-PD1 immunotherapy in hepatocellular carcinoma based on single-cell RNA sequencing. *Redox Biol.* (2022) 56:102463. doi: 10.1016/j.redox.2022.102463
- Lin J, Ruan W, Zhang J, Li H, Lu L. Exploring the role of ATF3 and ferroptosis-related RNA expression in osteoarthritis: An RNA analysis approach to immune infiltration. *Int J Biol Macromol.* (2024) 283:137872. doi: 10.1016/j.ijbiomac.2024.137872
- Liu X, Wei Q, Lu L, Cui S, Ma K, Zhang W, et al. Immunomodulatory potential of mesenchymal stem cell-derived extracellular vesicles: Targeting immune cells. *Front Immunol.* (2023) 14:1094685. doi: 10.3389/fimmu.2023.1094685
- Duraisamy K, Singh K, Kumar M, Lefranc B, Bonnafé E, Treilhou M, et al. P17 induces chemotaxis and differentiation of monocytes via MRGPRX2-mediated mast cell-line activation. *J Allergy Clin Immunol.* (2022) 149:275–91. doi: 10.1016/j.jaci.2021.04.040
- Qin S, Sun D, Li H, Li X, Pan W, Yan C, et al. The effect of SHH-gli signaling pathway on the synovial fibroblast proliferation in rheumatoid arthritis. *Inflammation.* (2016) 39:503–12. doi: 10.1007/s10753-015-0273-3

45. Clark JF, Soriano P. Diverse Fgfr1 signaling pathways and endocytic trafficking regulate mesoderm development. *Genes Dev.* (2024) 38:393–414. doi: 10.1101/gad.351593.124
46. Song H, Du H, Li J, Wang M, Wang J, Ju X, et al. Effect of fibroblast growth factor 2 on degenerative endplate chondrocyte: From anabolism to catabolism. *Exp Mol Pathol.* (2021) 118:104590. doi: 10.1016/j.yexmp.2020.104590
47. Tway CL, Filip SV. Catalysis at the crossroads. *Sci (1979).* (2025) 388:29–30. doi: 10.1126/science.adw5529
48. Ru Q, Li Y, Xie W, Ding Y, Chen L, Xu G, et al. Fighting age-related orthopedic diseases: focusing on ferroptosis. *Bone Res.* (2023) 11:12. doi: 10.1038/s41413-023-00247-y
49. Yao X, Sun K, Yu S, Luo J, Guo J, Lin J, et al. Chondrocyte ferroptosis contribute to the progression of osteoarthritis. *J Orthop Translat.* (2021) 27:33–43. doi: 10.1016/j.jot.2020.09.006
50. Gao YH, Zhao CW, Liu B, Dong N, Ding L, Li YR, et al. An update on the association between metabolic syndrome and osteoarthritis and on the potential role of leptin in osteoarthritis. *Cytokine.* (2020) 129:155043. doi: 10.1016/j.cyto.2020.155043
51. Coveney CR, Zhu L, Miotla-Zarebska J, Stott B, Parisi I, Batchelor V, et al. Role of ciliary protein intraflagellar transport protein 88 in the regulation of cartilage thickness and osteoarthritis development in mice. *Arthritis Rheumatol.* (2022) 74:49–59. doi: 10.1002/art.41894
52. Meng H, Fu S, Ferreira MB, Hou Y, Pearce OM, Gavara N, et al. YAP activation inhibits inflammatory signalling and cartilage breakdown associated with reduced primary cilia expression. *Osteoarthritis Cartilage.* (2023) 31:600–12. doi: 10.1016/j.joca.2022.11.001
53. Zhao S, Cheng L, Shi Y, Li J, Yun Q, Yang H. MIEF2 reprograms lipid metabolism to drive progression of ovarian cancer through ROS/AKT/mTOR signaling pathway. *Cell Death Dis.* (2021) 12:18. doi: 10.1038/s41419-020-03336-6
54. Chen DQ, Xie Y, Cao LQ, Fleishman JS, Chen Y, Wu T, et al. The role of ABCG10/MRP7 in anti-cancer drug resistance and beyond. *Drug Resistance Updates.* (2024) 73:101062. doi: 10.1016/j.drug.2024.101062
55. Chen X, Kang R, Kroemer G, Tang D. Broadening horizons: the role of ferroptosis in cancer. *Nat Rev Clin Oncol.* (2021) 18:280–96. doi: 10.1038/s41571-020-00462-0
56. Ragipoglu D, Dudeck A, Haffner-Luntzer M, Voss M, Kroner J, Ignatius A, et al. The role of mast cells in bone metabolism and bone disorders. *Front Immunol.* (2020) 11:163. doi: 10.3389/fimmu.2020.00163
57. Plum T, Feyerabend TB, Rodewald HR. Beyond classical immunity: Mast cells as signal converters between tissues and neurons. *Immunity.* (2024) 57:2723–36. doi: 10.1016/j.immuni.2024.11.016
58. Xiao P, Han X, Huang Y, Yang J, Chen L, Cai Z, et al. Reprogramming macrophages via immune cell mobilized hydrogel microspheres for osteoarthritis treatments. *Bioact Mater.* (2024) 32:242–59. doi: 10.1016/j.bioactmat.2023.09.010
59. Xu W, Zhang B, Xi C, Qin Y, Lin X, Wang B, et al. Ferroptosis plays a role in human chondrocyte of osteoarthritis induced by IL-1 β . *In Vitro Cartilage.* (2023) 14:455–66. doi: 10.1177/19476035221142011